A 5-DOF CABLE DRIVEN PARALLEL ROBOT FOR THE CALIBRATION OF RADIOTHERAPY MACHINES

Ramin Mersi[1], Louis Archambault[2], François Therriault-Proulx[3] , Philippe Cardou[1]
[1]*Laboratoire de robotique, Département de génie mécanique, Université Laval, Québec, QC, Canada*
Email: ramin.mersi.1@ulaval.ca; philippe.cardou@gmc.ulaval.ca
[2]*Département de Physique, de Génie Physique, Université Laval, Québec, QC, Canada*
Email: louis.archambault@phy.ulaval.ca
[3]*MedScint, Québec, QC, Canada*
Email: francois.tp@medscint.com

ABSTRACT

Water phantoms are critical tools for ensuring the accurate calibration of radiotherapy machines and effective treatments by using water as a medium for simulating human tissue. In this paper, we introduce a novel automated water phantom based on a 5-degree-of-freedom (5-DoF) cable-driven parallel robot. The system could offers several advantages over existing water phantoms, including faster movement and the ability to perform angular measurements due to its 90-degree continuous range of rotation. In order to determine the position of the cable attachment points on the end effector, we calculated the wrench-feasible workspace for all possible architectures of 5-DoF and 8 cables. Additionally, we developed an algorithm for determining whether there exists the continuous A-degree range of possible end-effector rotations in a prescribed $3A$-degree interval. With proper sampling, this algorithm enables the rapid elimination of architectures that do not cover the desired range of rotations. We also provide a detailed discussion of the robot design and construction, highlighting the features of the final built robot. Overall, our innovative water phantom design promises to be a new, efficient and precise method for the calibration of radiotherapy machines, and has the potential to improve patient outcomes in clinical practice.

Keywords: cable-driven parallel robot; water phantom; synthesis; radiotherapy.

ROBOT PARALLÈLE À CÂBLES DE 5 DEGRÉS DE LIBERTÉ POUR LA CALIBRATION DES MACHINES DE RADIOTHÉRAPIE

RÉSUMÉ

Les fantômes de test sont des outils essentiels pour assurer l'étalonnage précis des appareils de radiothérapie et ainsi assurer leur efficacité dans l'irradiation de tumeurs cancéreuses. Dans cet article, nous présentons un nouveau fantôme de test automatisé qui utilise un robot parallèle à câble à cinq degrés de liberté. Le système offre plusieurs avantages par rapport aux fantômes de test existants, notamment des déplacements plus rapides et la possibilité d'effectuer des mesures angulaires grâce à sa plage de rotations continues de 90 degrés. Pour déterminer les positions des points d'attache des câbles sur l'effecteur terminal, nous avons calculé l'espace de travail réalisable pour toutes les architectures possibles à cinq degrés de liberté et huit câbles. De plus, nous avons développé un algorithme général pour étudier la plage d'orientations continue de A degrés dans un intervalle de $3A$ degrés. Nous fournissons également une discussion détaillée de la conception et de la construction du robot, mettant en évidence les caractéristiques attendues du robot final construit. Dans l'ensemble, notre conception innovante du fantôme de test automatisé promet d'offrir une nouvelle méthode efficace et précise pour l'étalonnage des appareils de radiothérapie et a le potentiel d'améliorer les résultats sur les patients.

Mots-clés : robot parallèle entraîné par câble ; fantôme de test ; synthèse ; radiothérapie.

1. INTRODUCTION

1.1. Background

Phantoms are mainly used by medical physicists to emulate the human body properties in various medical treatments. These objects play a crucial role in radiation therapy for evaluating the prescribed doses, analyzing new radiation technologies in medical research, and calibrating radiotherapy machines (Fig. 1(a)). Phantoms can be broadly classified into two categories: solid phantoms and water phantoms. Solid phantoms are blocks of various materials that might be in the shape of different body organs, while a water phantom consists of a tank filled with water, which approximates the physics properties of muscles and other soft tissues. This is possible because water and soft tissues have similar radiation absorption and scattering properties, making water an effective stand-in for dose measurement in various positions.

Recent advance in scintillation detectors has greatly improved the accuracy of water phantom dosimetry [1]. However, despite this progress, human error remains a significant contributing factor to errors in radiotherapy treatment [2]. This is because the accuracy of dosimetry is dependent on both the accuracy of the dosimeter's position in the water tank and the accuracy of the dosimeter itself. To address this issue, recent research has focused on developing automated water phantoms that not only eliminate the potential for human error but also provide measurements at a far greater rate. To the knowledge of the authors, all the existing automated water phantoms use a simple Cartesian gantry mechanism to move the dosimeter inside the water tank, as shown in Fig. 1(b). Because their moving carriages perturb the water significantly, their speeds must be limited. Additionally, the use of aluminum in their arms and moving platforms introduces inaccuracy in radiation mapping. Cable robots, on the other hand, could be an ideal solution for moving a dosimeter in a water tank with minimum water and radiation disturbance, which should result in faster and more accurate measurements.

(a) (b)

Fig. 1. (a) A linear accelerator used in radio therapy at the CHU de Québec-Université Laval (b) Blue phantom2, one of the latest versions of automated water phantoms made by IBA company,at the CHU de Québec-Université Laval.

1.2. Literature Review

Two groups of papers are investigated for the scientific documentation review. First, papers related to water phantoms and available mechanisms for dosimetry; second, papers related to cable robots. In the

study by M. Konopacka et al. [3], a manual water tank was used to measure the amount of scattered dose during radiotherapy. The study utilized photon (6 MV) and electron (22 MeV) radiation distribution fields to measure the scattered dose at five different depths and three different locations in the water phantom. The manual water phantom used in this study required stopping the radiation and manually locating measurement cells at each desired position, which made the measurement process tedious and time-consuming. The use of an automated water tank could have enabled continuous and faster measurements. Hong et al. [4] compared radiological doses between water and solid phantoms at different depths, and noted that although the water phantom is more accurate, it has the disadvantage of taking a long time to perform a test and the possibility of human error during the implementation procedure. However, the newly introduced automated water tank in this paper overcomes these disadvantages. In a valuable paper by Akino et al. [5], the water phantom scanning systems of four major companies (IBA, PTW, Standard Imaging, and Sun Nuclear) were compared, and it was found that all of them provide adequate accuracy within 1% of the dose difference. While automated and semi-automated water phantoms are mostly commercial with limited published information, Hermann Fuchs et al. [6] published a paper that demonstrated the design of an innovative water phantom used for proton dosimetry in magnetic fields. Their design includes two stepper motors and an H-shaped belt-driven mechanism with two degrees of freedom, along with a high-precision Leica AT 402 laser tracker for position feedback of the ionization chamber. Their system achieves a positioning uncertainty of 0.16 mm with an absolute accuracy of 0.3 mm for complex movements. Despite these impressive results, the system has some limitations. Specifically, the existence of a moving bar in the middle of the mechanism can cause perturbations and slow down the scanning process. Additionally, the system is only suitable for measuring at specific depths.

Cable robots have found applications in various fields. Nan et al. [7] used a cable robot to position the receiver of a radio telescope, while Kite Robotics [8] developed a cable robot for cleaning windows on large buildings. The use of these robots is particularly advantageous when large workspaces are required. Additionally, the small volume occupied by the cables in this type of robot minimizes flow disturbance of the fluid where it operates. Lafourcade et al. [9] took advantage of this characteristic by using a cable robot to control the position and orientation of a model airplane in a wind tunnel. Moreover, some research has been conducted on cable-driven parallel robots to achieve wide ranges of rotations, such as those by Krut et al. [10] and by Zhang et al. [11]. It should be noted that these two robots are under-constrained and rely on gravity to maintain cable tension. In our case, however, an overconstrained robot will be necessary to keep the cables straight and optimize the robot's acceleration capabilities. In recent years, cable robots have found a growing number of applications in medical engineering. A noteworthy example of such use is in minimally invasive interventions, where Amaar Quadri et al. [12] employed an expandable cable-driven parallel mechanism.

In this paper, our objective is to develop a novel automated water phantom based on a cable-driven parallel robot. Because these robots can move fast with minimal perturbations of the fluid immersing them and because its moving parts can easily be non-metallic, they have the potential of providing more accurate scans in less time. By employing this approach, we aim to achieve faster and more precise radiation mappings, which would open new avenues of experimentation in the field of radiotherapy machines.

2. CONCEPTUAL DESIGN

The first phase of the design process is the conceptual design, which involves visualizing the idea and determining the key factors that will shape the design, such as the number of cables and the required number of degrees of freedom. The prototype will be constructed inside a box-shaped water tank with dimensions of 700 mm in length, 700 mm in width, and 560 mm in height. The required workspace by the medical physicists involved in the project is a cylindrical shape within the tank with a diameter and height of ap-

proximately 150 mm. The prototype must also have a wide range of tilt angles in addition to the three translational movements. The rotation of the moving platform around its own axis is not a critical aspect for this application, since the directional sensor it carries, a dosimeter, is not significantly affected by this motion. Therefore, the end effector is designed as a rod with five degrees of freedom for control, assuming the radius of the rod is negligible for the purposes of this study.

Due to the unidirectional nature of cables, cable robots require at least one more cable than their mobility for their moving platforms to be fully constrained without the action of gravity. In order to achieve 5 degrees of freedom, at least six cables are needed. However, due to the box shape of the water tank, it is decided to use eight cables, one cable anchored at each vertex. Workspace analyses with six and seven cables have led to relatively small workspaces in position and in rotation, while eight cables result generally in a larger symmetric workspace and wider ranges of rotations.

Another critical requirement for this robot is a high accuracy of at least 1 mm. However, due to the elastic nature of cables, achieving this level of accuracy is challenging in cable robots through the use of encoder feedback alone. Therefore, to overcome the limitations imposed by the elastic nature of cables, a non-contact sensor should be employed for precise position measurement in the inverse kinematic problem. The four common types of non-contact displacement measurement technology are Ultrasonic, optical, magnetic, and image processing. Ultrasonic sensors have a range of several meters and recent methods, such as amplitude modulation (AM) method, can achieve an accuracy of 0.02 mm within 0.5 meters [13]. However, their accuracy can be easily affected by environmental factors, such as temperature and humidity. Moreover, if they are located outside of the water tank, they may not work properly due to the changing environment from air to water. Magnetic sensors cannot be used due to the interference of their magnetic field with the radiation of the medical linear accelerator (LINAC); moreover, it is not supposed to use any metallic part on the end effector. The optical methods, specifically laser sensors promise to be the solution with the highest accuracy; however, due to the limited budget, it is decided to use image processing as the primary position feedback.

3. OPTIMUM GEOMETRIC DESIGN

Because we hypothesize that symmetry must be preserved in the cable arrangement to maximise the workspace volume, the fixed cable attachment points are constrained at the vertices of the water tank. This reduces the geometric design problem to that of determining the cable attachment points on the rod-shaped end effector. In doing so, we wish to completely cover the desired position workspace and maximize the range of rotations of the rod.

Again because of symmetry considerations, a total of three possible attachment points on the rod are considered: one at each end and one in the middle. Although the middle point might risk cable-cable and cable-EE interference, we included it for a thorough analysis. However, as shown at the end of this section, the final chosen configuration employs only the sides of the end-effector for cable connections.

Incorporating all three potential attachment points yields a total of $3^8 = 6561$ possible configurations for the attachment of the eight cables. However, certain configurations can be ruled out at the outset. For example, when eight cables connect at a common point the end-effector becomes a point mass, and its rotations cannot be controlled. In order to determine the most suitable configuration, a program is developed to trace the constant-orientation wrench feasible workspace (WFW) for the 5-DOF cable robot. All possible WFWs are then calculated for the various angles and geometries, and the solutions that satisfy the design constraints are retained. These steps will be discussed in greater detail in the following sections.

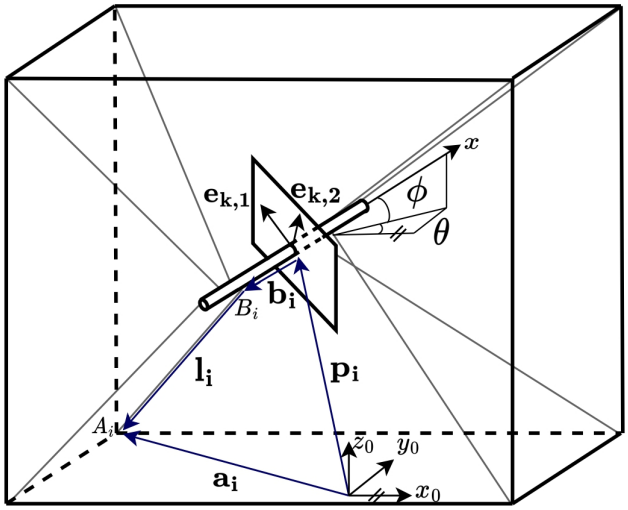

Fig. 2. Geometric schematic of a general 5-DoF cable-driven parallel robot

3.1. Geometric Model of a 5-DoF CDPR

While the geometric model of a CDPR is relatively straightforward, it is crucial to mention it thoroughly since it is essential for static modelling. Figure 2 represents a general 5-DoF CDPR which has a rod end-effector (EE). As discussed before, the fixed cable attachment points on the base are located at the vertices of a box-shaped frame. The mobile frame, which is fixed on the EE, is represented by the unit vector $\mathbf{x}$ parallel to the direction of the rod and two angles ϕ and θ representing the tilt and azimuthal angles respectively. Additionally, x_0, y_0 and z_0 are the axes of the fixed frame. $\mathbf{e}_{k,1}$ and $\mathbf{e}_{k,2}$ are two unit vectors which lie on the plane perpendicular to the rod and will be discussed in more details in the following section.

To develop a general geometric model, we assume that the cables are under tension and that spherical joints are present on both sides of the cables. This ensures that the points A_i and B_i are fixed with respect to the fixed and moving frames, respectively. As a result, the position vectors of A_i in the fixed frame and B_i in the mobile frame, denoted by $\mathbf{a}_i$ and $\mathbf{b}_i$, respectively, are independent of the pose of the EE. The position of the EE is represented by $\mathbf{p}$, and $\mathbf{l}_i$ is the cable vector pointing from the EE towards the frame. By applying a vector loop to a random cable i, we obtain:

$$\mathbf{l}_i = \mathbf{a}_i - \mathbf{R}\mathbf{b}_i - \mathbf{p} \quad \text{for } i = 1, ..., 8 \tag{1}$$

where $\mathbf{R}$ is the rotation matrix, which can be represented as ϕ rotation around y_0 and afterwards a θ rotation around z_0, leading to the following equation:

$$\mathbf{R} = \mathbf{R}_{z_0,(\theta)}\mathbf{R}_{y_0,(\phi)} = \begin{bmatrix} \cos(\theta)\cos(\phi) & -\sin(\theta) & \cos(\theta)\sin(\phi) \\ \sin(\theta)\cos(\phi) & \cos(\theta) & \sin(\theta)\sin(\phi) \\ -\sin(\phi) & 0 & \cos(\phi) \end{bmatrix} \tag{2}$$

Furthermore, the unit vector of the cables pointing from the EE towards the base is denoted as:

$$\mathbf{u}_i = \frac{\mathbf{l}_i}{\|\mathbf{l}_i\|_2} \tag{3}$$

which will be used in the following section to demonstrate the direction of the tensions in the cables. Eventually, it is worth mentioning that by calculating the second norm of Eq. (1), the inverse kinematics function can be simply obtained.

3.2. Wrench Feasible Workspace for 5DoF CDPRs

The concept of WFW is a critical aspect of the design and control of CDPRs. It characterises the ability of the robot to reach a set of desired poses under prescribed cable tension limits. In order to determine the WFW, it is necessary to first establish the static equilibrium conditions of the robot end effector. The general equation for the mechanical equilibrium of a moving platform with m cables and six degrees of freedom is represented as

$$\mathbf{W}\mathbf{t} = -\mathbf{w}_e, \tag{4}$$

where $\mathbf{W}$ is the wrench matrix and represents the transpose of the robot Jacobian matrix, $\mathbf{t}$ is the vector of cable tensions, and $\mathbf{w}_e$ is the wrench resulting from the external forces acting on the moving platform. As illustrated in Fig. 2, the cable robot being discussed in this paper comprises eight cables which allows us to rewrite Eq. (4) as

$$\begin{bmatrix} \mathbf{u}_1 & \cdots & \mathbf{u}_8 \\ \mathbf{b}_1 \times \mathbf{u}_1 & \cdots & \mathbf{b}_8 \times \mathbf{u}_8 \end{bmatrix} \begin{bmatrix} t_1 \\ t_2 \\ \vdots \\ t_8 \end{bmatrix} = - \begin{bmatrix} \mathbf{f} \\ \tau \end{bmatrix}, \tag{5}$$

where $\mathbf{f}$ and τ denote the force and torque vectors acting along the $[x_0, y_0, z_0]$ axes, and f_i denotes the tension in cable i. Because the EE has the shape of a straight rod, all cable tensions intersect a common line, and matrix $\mathbf{W}$ is rank-deficient. In order to work with a full-rank 5×8 matrix, a transformation matrix $\mathbf{S} \in \mathbb{R}^{5\times 6}$ needs to be found that can be used to eliminate the moment acting along the rod. Upon multiplying both sides of Eq. (4) with $\mathbf{S}$, we obtain:

$$\mathbf{S}\mathbf{W}\mathbf{t} = -\mathbf{S}\mathbf{w}_e \tag{6}$$

The $\mathbf{S}$ matrix should only affect the torque components and will project them onto a plane perpendicular to the rod. It takes the form

$$\mathbf{S} = \begin{bmatrix} \mathbf{1}_{3\times 3} & \mathbf{0}_{3\times 3} \\ \mathbf{0}_3^T & \mathbf{e}_{k,1}^T \\ \mathbf{0}_3^T & \mathbf{e}_{k,2}^T \end{bmatrix}, \tag{7}$$

where $\mathbf{e}_{k,1}^T$ and $\mathbf{e}_{k,2}^T$ are two arbitrary unit vectors perpendicular to the rod and to each other. Assuming $\mathbf{e} = [e_x \; e_y \; e_z]^T$ is the unit vector parallel to the rod, we have

$$\mathbf{e} \perp \mathbf{e}_{k,1}^T \Rightarrow \mathbf{e}^T \mathbf{e}_{k,1} = 0 \quad \text{and} \quad \mathbf{e} \times \mathbf{e}_{k,1} = \mathbf{e}_{k,2} \tag{8}$$

The selection of two arbitrary components for $\mathbf{e}_{k,1}$ allows for the determination of the third component through first part of Eq. (8). However, if the corresponding third component in $\mathbf{e}$ is zero, then the $\mathbf{e}_{k,1}$ variable cannot be determined. To circumvent this issue, the maximum component of $\mathbf{e}$ is first identified, and the corresponding variable in $\mathbf{e}_{k,1}$ is set as the unknown, while the remaining two are chosen arbitrarily, as follows:

$$\mathbf{e}_{k,1} = \begin{cases} \frac{1}{\sqrt{2+\left(\frac{e_y+e_z}{e_x}\right)^2}} \begin{bmatrix} -\frac{e_y+e_z}{e_x} & 1 & 1 \end{bmatrix}^T & \text{if } \max(e_x, e_y, e_z) = e_x \\ \frac{1}{\sqrt{2+\left(\frac{e_x+e_z}{e_y}\right)^2}} \begin{bmatrix} 1 & -\frac{e_x+e_z}{e_y} & 1 \end{bmatrix}^T & \text{if } \max(e_x, e_y, e_z) = e_y \\ \frac{1}{\sqrt{2+\left(\frac{e_x+e_y}{e_z}\right)^2}} \begin{bmatrix} 1 & 1 & -\frac{e_x+e_y}{e_z} \end{bmatrix}^T & \text{if } \max(e_x, e_y, e_z) = e_z \end{cases} \tag{9}$$

The vector $\mathbf{e}_{k,2}$ can then be computed from $\mathbf{e}_{k,1}$ through the second part of Eq. (8).

Eventually, the hyperplane shifting method, first proposed by Bouchard et al. [14], is employed to determine the WFW of the cable-driven parallel robot under examination. The wrench set is represented by a 5-dimensional polytope, which is bounded by 4-dimensional facets. To proceed, the 4-dimensional facets of the 8-dimensional polytope of feasible tensions are projected onto the five-dimensional wrench space. If the projected polytope, which is derived from the feasible tensions, is fully contained in the prescribed wrench set, then the calculated pose is deemed feasible. The prescribed wrench set represents the external forces and torques that the robot is expected to encounter during operation, and can be determined based on the robot's intended use case and environment.

3.3. Finding The Optimum Geometry

In our application, the optimum CDPR geometry is that which allows to move the rod EE across the full 90° range of tilt angles, i.e., $\phi \in [\phi_0 - 45^\circ, \phi_0 + 45^\circ]$. The offset angle ϕ_0 can be chosen freely, since the only requirement is assumed to be a continuous 90° range of tilt angles, not a definite set of orientations of the EE. Notice also that the other orientation parameter θ can vary freely while the rod covers its required range of tilt angles ϕ. Nevertheless, in order to compare the range of ϕ angles across different architectures in this study, we have set θ to be 45°. This decision is dictated by the geometry of the cubic water tank. When θ is set to 45°, the rod aligns with the tank diagonal, allowing for the maximum possible range of ϕ.

In order to determine the optimal geometry for our application, the force limitations of the cables must first be established. The maximum tension in the cables, as determined by the motor, reductor and drum size used in the robot, is set at 20 N and the minimum tension in each cable is set at 1 N to prevent sagging. Wrench-feasibility can then be determined, for a given pose of the moving platform, by solving the following constraint-satisfaction problem:

$$\begin{cases} \mathbf{W}\mathbf{t} = -\mathbf{w}_e \\ \mathbf{1}_8 \text{ N} \leq \mathbf{t} \leq 20 \cdot \mathbf{1}_8 \text{ N} \end{cases} \tag{10}$$

where $\mathbf{1}_8$ is the eight-dimensional array of ones. A program must then be developed to calculate the WFW for all possible geometries and for different angles of each of them. The design constraints include a cylindrical WFW with a height and a diameter of 150 mm, as well as a continuous 90°-range of rotation. To evaluate whether the prescribed 90°-range of tilt angles is covered, we must verify wrench feasibility for a sample of tilt angles ϕ. The question that arises is how many angles and which angles of each architecture should the constant-orientation WFW be traced for. This question is important because of the large number of CDPR geometries under consideration.

Due to the symmetric architecture of the water tank, it is sufficient to investigate the tilt angles between -90° to 90° (half circle); the behaviour of the robot being the same in the $[-180^\circ, -90^\circ]$ and $[90^\circ, 180^\circ]$ ranges. Therefore, if the bisector ϕ_0 of our 90° desired range can rotate from -90° to 90°, the range of rotations that should be considered extends from -135° to 135°. We must now define an efficient order selection of angles to verify various tilt angles ϕ within this 270°-range. To achieve this, we propose a pruning algorithm that resembles the bisection method. It aims to eliminate the architectures that do not possess the desired continuous rotation range, leaving the validation of the remaining geometries for a later stage. The method involves a series of steps, beginning with the generation of a pair of angles. If the WFW of each angle in the pair includes the desired cylindrical workspace, the method proceeds to the next step. It consists in generating another pair of angles, at half the distance to its neighboring angles. This method can be used as a general approach to identify a continuous A° range of rotation within a $3A^\circ$ space and the

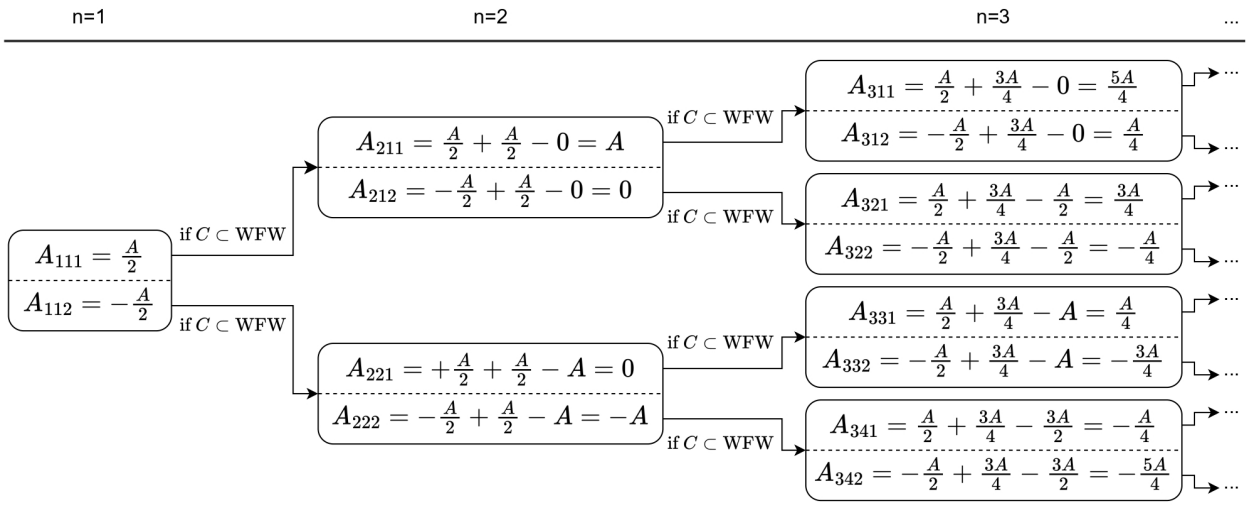

Fig. 3. The first three steps of the angle selection process for a continuous A-degree

formula for each pair is as follows:

$$A_{njk} = \begin{cases} (-1)^{k-1}\frac{A}{2} & \text{for } n = 1 \\ (-1)^{k-1}\frac{A}{2} + \sum_{i=1}^{n-1} \frac{A}{2^i} - (j-1)\frac{A}{2^{n-2}} & \text{for } n \geq 2 \end{cases} \tag{11}$$

In this expression, A_{njk} denotes the k^{th} angle in the j^{th} pair at the n^{th} step. In each pair of j, there are just two angles k=1 and k=2. Figure 3 illustrates the first three steps of the angle selection process, where C is the desired workspace and the nomenclature of n, j, and k is self-explanatory. It is important to note that these are the maximum number of angles that could be selected, and any angle that does not satisfy the desired workspace ($C \not\subset$WFW) will not be considered for the next step. Additionally, it is clear that the j^{th} pair in each step is created by the j^{th} angle of the previous step (for $n \geq 2$). In general, in each step, there would be 2^{n-1} pairs which are equivalent to 2^n angles. However, since the difference between the upper and lower angles in each pair is equal to the desired range (A), it is determined that in each step, the second angles in the first half of the pairs are the same as the first angles of the second half pairs. This means that for $n = 3$, $A_{312} = A_{331}$ and $A_{322} = A_{341}$, as shown in Fig. 3. As a result, the maximum number of angles that need to be investigated in each step is $3 \times 2^{n-2}$ for $n \geq 2$. For illustrative purposes, let us consider our specific goal: to find a continuous 90° rotation within a 270° range. Applying the formula, in the first step, we need to determine the WFW for angles at $+45°$ and $-45°$. If neither angle yields a result, we can confidently conclude that the investigated architecture does not support our desired 90° range of rotation. However, if either $+45°$ or $-45°$ does yield a result, we proceed to the second step. Here, for the $+45°$ angle, we would investigate angles at 90° and 0°. Simultaneously, for the $-45°$ angle, we would explore angles at 0° and $-90°$. Thus, by persisting with this process, we can efficiently eliminate many architectures that are unable to provide the desired continuous rotation range, and this is achieved by computing the WFW for just a limited set of angles.

A MATLAB program was then developed to compute the WFW for all possible architectures. To evaluate whether the cylinder is fully included inside the WFW for a given ϕ of an architecture, we approximate the desired cylinder workspace to a cube with 150 mm edges. We then discretise the cube into $10 \times 10 \times 10$ EE poses, and evaluate a kinetostatic index called the minimum degree of constraint satisfaction index [15] at each of these poses. The points that have a positive index are deemed wrench feasible. Therefore, the

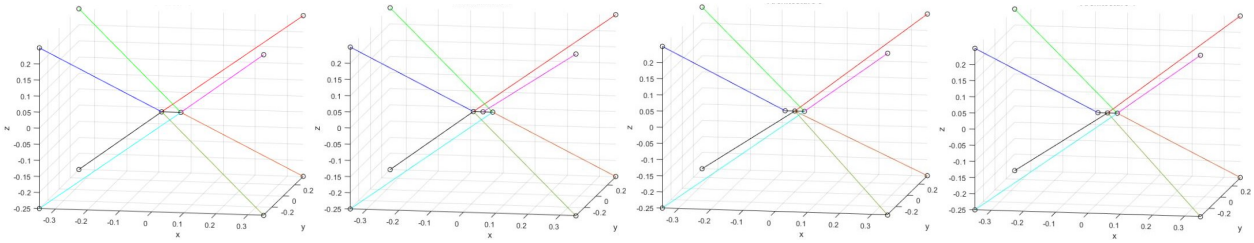

(a) (b) (c) (d)

Fig. 4. The four architectures that satisfy the design constraints.

inclusion $C \subset \text{WFW}$ is considered to hold true when all the poses in the cubic mesh correspond to positive values of the kinetostatic index. Calculating the WFW for all the tilt angles obtained from the aforementioned formula revealed that through the first four steps of the algorithm, a majority of the architectures were eliminated, resulting in a total of 44 remaining architectures. Next, the cable-cable interference was considered, and the interference-free workspace of the architectures was investigated using the geometrical method introduced by Perreault et al. [16]. Additionally, due to the symmetric shape of the frame, certain architectures exhibited equivalent geometries, which were subsequently omitted. As a result, only four architectures remained, which are relatively similar to each others, as can be appreciated in Fig. 4.

Ultimately, the architecture shown in Fig. 4(a) was chosen as the optimal design due to its more symmetrical workspace compared to those of the other three. In Figs. 5 and 6, the WFW of the architectures shown in Figs. 4(a) and 4(d) are depicted for three different tilt angles of $-10°$, $35°$, and $80°$.

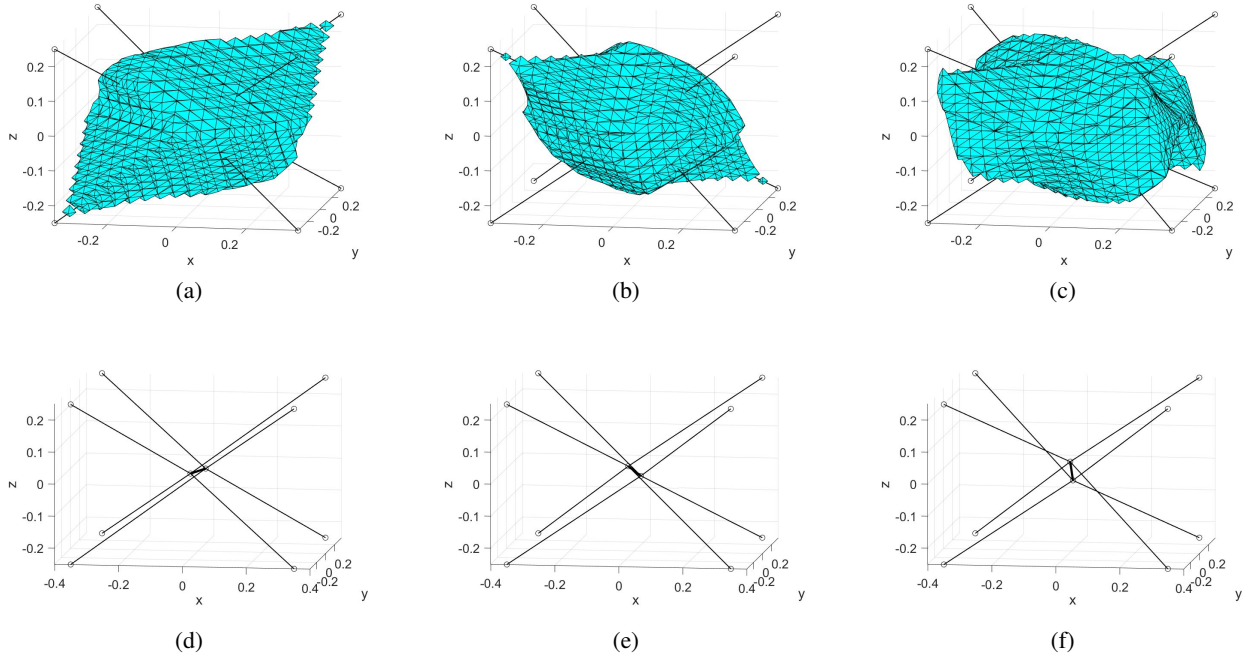

(a) (b) (c)

(d) (e) (f)

Fig. 5. Tracing WFW of the selected architecture for $\theta = 45°$ and 3 tilt angles of the EE: (a)$\phi = -10°$, (b)$\phi = 35°$ and (c)$\phi = 80°$; (d), (e), and (f) depict the architecture for $\theta = 45°$ and $-10°$, $35°$, and $80°$ tilt angles respectively.

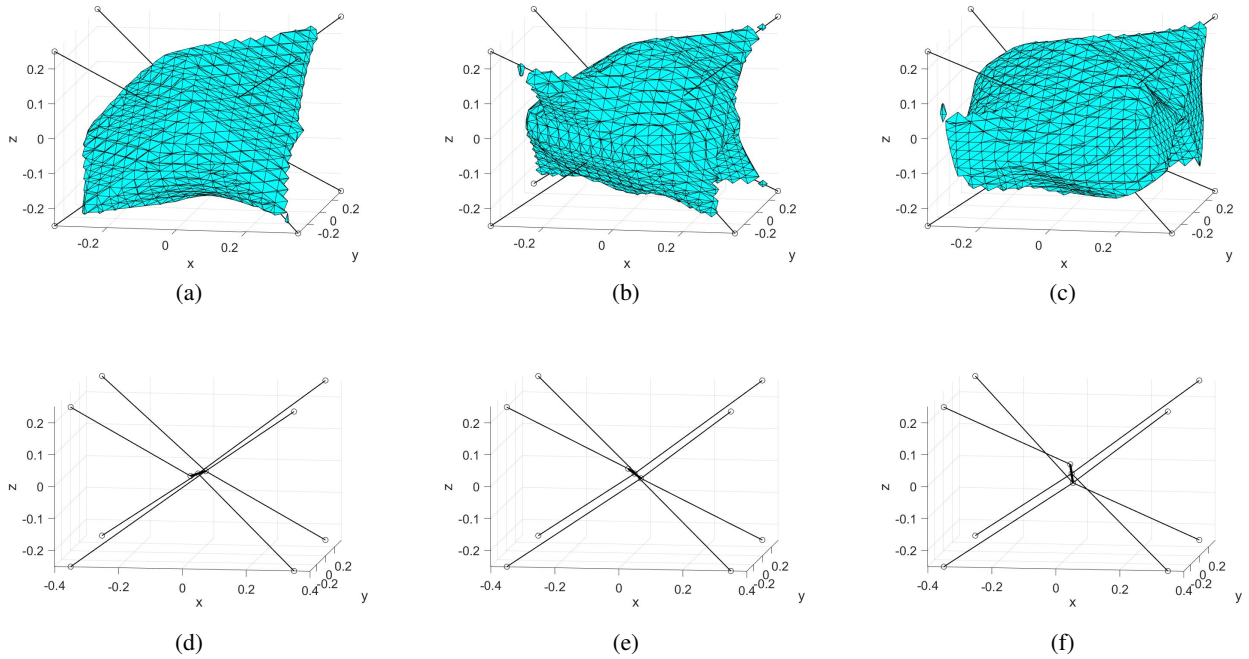

Fig. 6. Tracing WFW of the architecture shown in Fig. 4(d) for $\theta = 45^\circ$ and 3 tilt angles of the EE: (a)$\phi = -10^\circ$, (b)$\phi = 35^\circ$ and (c)$\phi = 80^\circ$; (d), (e), and (f) depict the architecture for $\theta = 45^\circ$ and -10°, 35°, and 80° tilt angles respectively.

4. DETAILED DESIGN

The design of the robot can be divided into three distinct steps. The first step entailed determining the appropriate location for the winches and the routing of the cables. The second stage focused on the design of the winch system for winding and unwinding the cables. The final stage involved the design of the swivel pulleys.

In the initial stage of the design process, it was determined to position four winches on the right and the other four on the left side of the water tank. Due to limited space on each side, the winches were arranged on shelves stacked on top of one another. The eight cables were then redirected to the top of the water tank, with four of them passing through upper swivel pulleys located outside of the water, and the remaining four cables routed to swivel pulleys located at the bottom of the tank within the water. Additionally, due to the relatively low stiffness of the polymethyl methacrylate (PMMA) material used to construct the water tank, an aluminum structure was added both inside and outside of the tank to increase its stiffness. This helps to minimize vibrations caused by the motion of the robot and prevents deformation of the tank under the continuous stress of the cables.

The design of the winches was adapted from a mechanism previously presented by R. Mersi et al. [17] and further developed by F. Centomo et al. [18]. As depicted in Fig. 7, an exploded view of one of the winches is presented. The design incorporates a drum that rotates as a result of the movement of three rods connected to a motor through a coupling. A lead screw, located at the center of the drum, is fully constrained and allows for simultaneous translational movement as the drum rotates. The pitch of the lead screw is matched to that of the drum, ensuring that the cable attachment point remains fixed.

In the final design phase, the swivel pullies were carefully considered. For the upper swivel pullies, which receive the cables horizontally, the center of mass was placed on the horizontal line of the cable to ensure

No.	Component
1	Actuator
2	Strengthen Aluminium Rod
3	Coupling
4	Ball Bearing
5	Acrylic Resin Cover
6	Ball Bearing
7	Lead Screw Nut
8	Aluminium Drum
9	Stainless Steel Lead Screw
10	Precise Stainless Steel Rod
11	Limit Switch
12	Limit Switch Holder
13	Pulley Holder
14	Pulley
15	Bracket

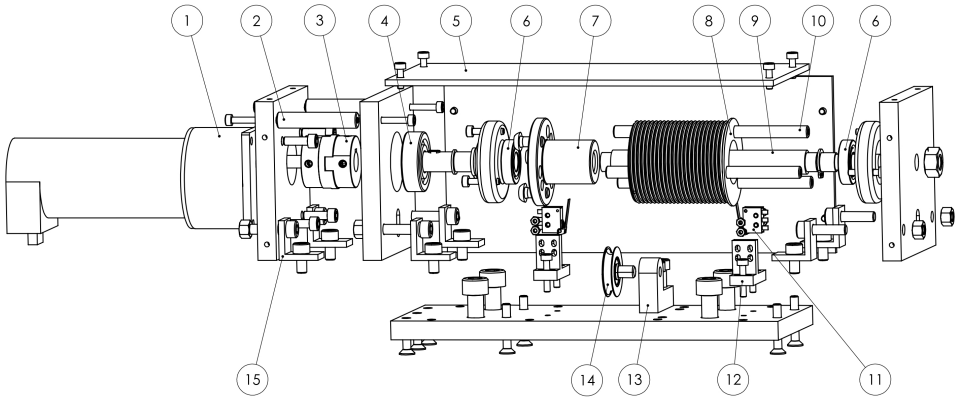

Fig. 7. Exploded view of the designed winch system.

rotations independent from gravitational forces. However, for the lower swivel pullies, which receive the cables vertically, this balancing was unnecessary. Instead, the focus was on selecting components that were resistant to water damage as they are located within the water tank.

In addition to the design considerations mentioned above, cable selection is also an important criterion for designing a CDPR. The cable should have a high stiffness to allow accurate feedback from the encoders and low creep for better repeatability. Commonly used synthetic fibers in cable robots include polyester, Aramid (Kevlar), UHMWPE (Dyneema), and Vectran. In this project, Vectran cable was selected due to its

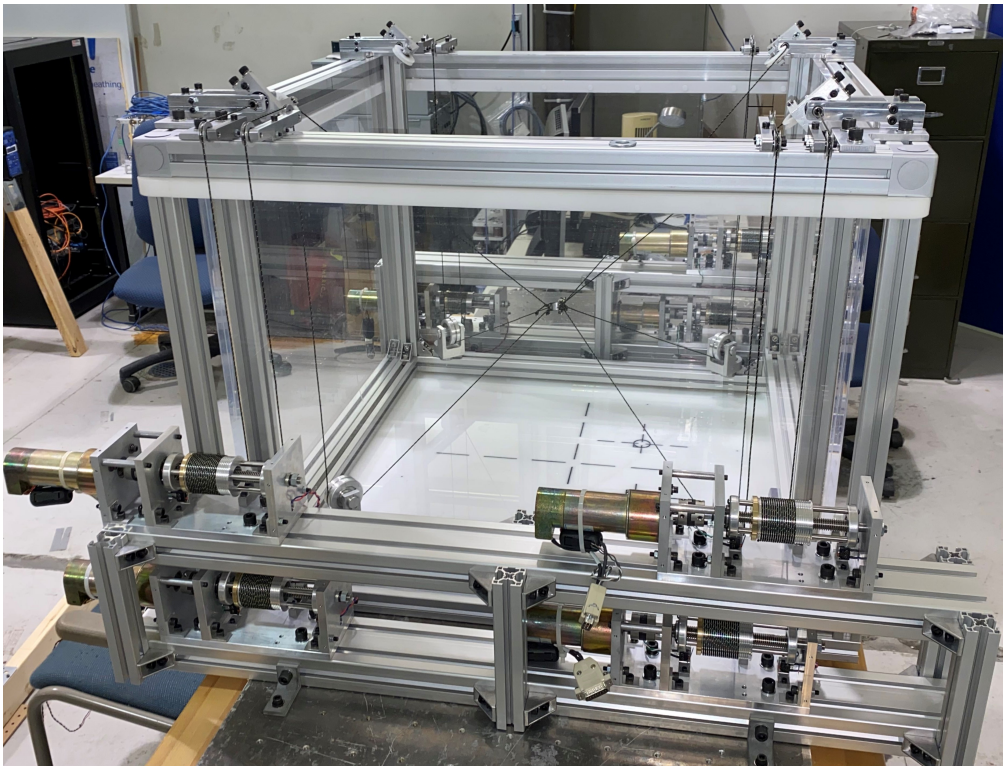

Fig. 8. The cable-driven water phantom in the Laboratoire de Robotique at Université Laval

low elongation and creep [19], as well as its high resistance to moisture compared to other possible options. Therefore, a 1.5 mm diameter Vectran cable with an average break load of 119 kg was chosen.

Incorporating the design considerations mentioned above, as well as careful cable selection, the completed assembly of the robot can be seen in Fig. 8.

5. CONCLUSION

In conclusion, this paper presents a novel automated water phantom that uses a cable-driven parallel robot in order to carry a dosimeter for calibrating radiotherapy machines. The presented CDPR design was obtained by an exhaustive search of the CDPRs with eight cables stemming from the eight vertices of the water tank and attaching at three collinear points on the dosimeter. It promises to offer advantages over existing models, including faster scanning rate and a wider range of measurements due to its 90-degree continuous tilt angle. The next steps will consist assessing the accuracy and speed of the apparatus, and possibly to implement a contactless extrinsic source of measurement of the dosimeter pose inside the water tank.

ACKNOWLEDGEMENTS

The authors dutifully acknowledge the support of NSERC for this research through the CREATE grant #498011.

REFERENCES

1. Uijtewaal, P., Côté, B., Foppen, T., de Vries, J.H.W., Woodings, S.J., Borman, P.T.S., Lambert-Girard, S., Therriault-Proulx, F., Raaymakers, B.W. and Fast, M.F. "Performance of the hyperscint scintillation dosimetry research platform for the 1.5 t mr-linac." *Physics in Medicine & Biology*. ISSN 0031-9155. doi:10.1088/1361-6560/acb30c, 2 2023.
2. Ibbott, G.S., Haworth, A. and Followill, D.S. "Quality assurance for clinical trials." *Frontiers in Oncology*, Vol. 3. ISSN 2234-943X. doi:10.3389/fonc.2013.00311, 2013.
3. Konopacka, M., Rogoliński, J. and Ślosarek, K. "Direct and bystander effects induced by scattered radiation generated during penetration of radiation inside a water-phantom." *Mutation Research/Genetic Toxicology and Environmental Mutagenesis*, Vol. 721, pp. 6–14. ISSN 13835718. doi:10.1016/j.mrgentox.2010.11.013, 3 2011.
4. Hong, J., Lee, H. and Cho, J. "Comparison of the photon charge between water and solid phantom depending on depth." *International Journal of Radiation Research*, Vol. 13, pp. 229–234, 7 2015.
5. Akino, Y., Gibbons, J.P., Neck, D.W., Chu, C. and Das, I.J. "Intra- and intervariability in beam data commissioning among water phantom scanning systems." *Journal of Applied Clinical Medical Physics*, Vol. 15, pp. 251–258. ISSN 1526-9914. doi:10.1120/jacmp.v15i4.4850, 7 2014.
6. Fuchs, H., Padilla-Cabal, F., Hummel, A. and Georg, D. "Technical note: Design and commissioning of a water phantom for proton dosimetry in magnetic fields." *Medical Physics*, Vol. 48, pp. 505–512. ISSN 0094-2405. doi:10.1002/mp.14605, 1 2021.
7. NAN, R., LI, D., JIN, C., WANG, Q., ZHU, L., ZHU, W., ZHANG, H., YUE, Y. and QIAN, L. "The five-hundred-meter aperture spherical radio telescope (fast) project." *International Journal of Modern Physics D*, Vol. 20, pp. 989–1024. ISSN 0218-2718. doi:10.1142/S0218271811019335, 6 2011.
8. "Kite robotics." `https://www.kiterobotics.com/en`. Accessed: 2023-03-07.
9. Lafourcade, P., Llibre, M. and Reboulet, C. "Design of a parallel wire-driven manipulator for wind tunnels." pp. 187–194, 2002.
10. Krut, S., Ramdani, N., Gouttefarde, M., Company, O. and Pierrot, F. "A parallel cable-driven crane for scara-motions." pp. 101–108. ASMEDC. ISBN 978-0-7918-4326-0. doi:10.1115/DETC2008-49969, 1 2008.
11. Zhang, Z., Shao, Z., Wang, L. and Shih, A.J. "Optimal design of a high-speed pick-and-place cable-driven parallel robot." doi:10.1007/978-3-319-61431-1_29, 2018.
12. Quadri, A., Zhou, J., Sewani, A. and Tavallaei, M.A. "Parameter estimation and tracking of an expandable

cable-driven parallel mechanism for minimally invasive interventions." *IEEE Transactions on Medical Robotics and Bionics*, Vol. 4, pp. 414–422. ISSN 2576-3202. doi:10.1109/TMRB.2022.3161065, 5 2022.
13. Qiu, Z., Lu, Y. and Qiu, Z. "Review of ultrasonic ranging methods and their current challenges." *Micromachines*, Vol. 13, p. 520. ISSN 2072-666X. doi:10.3390/mi13040520, 3 2022.
14. Bouchard, S., Gosselin, C. and Moore, B. "On the ability of a cable-driven robot to generate a prescribed set of wrenches." *Journal of Mechanisms and Robotics*, Vol. 2. ISSN 1942-4302. doi:10.1115/1.4000558, 2 2010.
15. Guay, F., Cardou, P., Cruz-Ruiz, A.L. and Caro, S. "Measuring how well a structure supports varying external wrenches." doi:10.1007/978-94-007-7485-8_47, 2014.
16. Perreault, S., Cardou, P., Gosselin, C.M. and Otis, M.J.D. "Geometric determination of the interference-free constant-orientation workspace of parallel cable-driven mechanisms." *Journal of Mechanisms and Robotics*, Vol. 2. ISSN 1942-4302. doi:10.1115/1.4001780, 8 2010.
17. Mersi, R., Vali, S., Abbasnejad, G. and Masouleh, M.T. "Design and control of a suspended cable-driven parallel robot with four cables." pp. 470–475. ISBN 9781728101279. doi:10.1109/ICRoM.2018.8657534, 2018.
18. Centomo, F., Savegnago, Y., Jovanovic, N. and Zuffellato, L. "Progettazione di un winch per robot a cavi.", 2022.
19. Nanthacoumarane, S., Wang, B., Kouadri-Henni, A., Cardou, P. and Caro, S. "Polymer cable characterization in cable-driven parallel robots.", 2022.